# UCLA
## UCLA Previously Published Works

**Title**
Biomechanical Consequences of Rapid Evolution in the Polar Bear Lineage

**Permalink**
https://escholarship.org/uc/item/9967f2k4

**Journal**
PLOS ONE, 5(11)

**ISSN**
1932-6203

**Authors**
Slater, Graham J
Figueirido, Borja
Louis, Leeann
et al.

**Publication Date**
2010

**DOI**
10.1371/journal.pone.0013870

**Copyright Information**

Peer reviewed

PLoS one

# Biomechanical Consequences of Rapid Evolution in the Polar Bear Lineage

Graham J. Slater[1]*, Borja Figueirido[2], Leeann Louis[3], Paul Yang[1], Blaire Van Valkenburgh[1]

1 Department of Ecology and Evolutionary Biology, University of California Los Angeles, Los Angeles, California, United States of America, 2 Departamento de Ecología y Geología, Área de Paleontología, Facultad de Ciencias, Universidad de Málaga, Campus Universitario de Teatinos, Málaga, Spain, 3 Cornell University Museum of Vertebrates, Ithaca, New York, United States of America

## Abstract

The polar bear is the only living ursid with a fully carnivorous diet. Despite a number of well-documented craniodental adaptations for a diet of seal flesh and blubber, molecular and paleontological data indicate that this morphologically distinct species evolved less than a million years ago from the omnivorous brown bear. To better understand the evolution of this dietary specialization, we used phylogenetic tests to estimate the rate of morphological specialization in polar bears. We then used finite element analysis (FEA) to compare the limits of feeding performance in the polar bear skull to that of the phylogenetically and geographically close brown bear. Results indicate that extremely rapid evolution of semi-aquatic adaptations and dietary specialization in the polar bear lineage produced a cranial morphology that is weaker than that of brown bears and less suited to processing tough omnivorous or herbivorous diets. Our results suggest that continuation of current climate trends could affect polar bears by not only eliminating their primary food source, but also through competition with northward advancing, generalized brown populations for resources that they are ill-equipped to utilize.

## Introduction

The polar bear *Ursus maritimus* is unique among living ursids as the only member of the family with an exclusively carnivorous diet. As a result of this specialized diet, the the polar bear has evolved a series of craniodental adaptations that allow it to efficiently process a diet of seal flesh and blubber. For example, polar bears exhibit reduced surface area of the grinding molar teeth, a feature normally pronounced in more omnivorous ursids, and a low, slender skull [1], [2]. Despite possessing such distinctive phenotypic features, molecular and paleontological data unequivocally indicate that the carnivorous polar bear evolved relatively recently, approximately 150–700ka (Fig. 1), from coastal populations of the more generalized and omnivorous brown bear *Ursus arctos* [3–6]. In this study, we take a combined evolutionary and biomechanical approach to examine the evolution of adaptations to carnivory in the polar bear cranium. We first use multivariate evolutionary contrasts [7] to test whether the unique cranial morphology of the polar bear resulted from increased rates of cranial shape evolution in the polar bear lineage, relative to other branches of ursid phylogeny. We expect this to be the case if adaptation to the harsh arctic environment and a hypercarnivorous diet posed novel evolutionary challenges for a large ursid. We then use 3D finite element analysis (FEA) to examine the impact of craniodental adaptations to hypercarnivory on various aspects of cranial performance, such as bite force and skull strength, during feeding. FEA is an engineering method used to examine patterns of stress and strain in man-made objects when placed under load and, in recent years, has been adapted to study the evolution of

biological form and function [8–14]. In FEA, the structure of interest, here the skull, is represented as a finite number of elements, joined at their vertices by nodes. The elements are assigned material properties that specify how they respond when placed under load. Recent developments in FE modeling of biological structures have resulted in methods for more realistic modeling of jaw muscles [15] and appropriate protocols for assessing comparative performance across species [16]. Here, we use FEA to compare feeding performance in the carnivorous polar bear to that of its phylogenetically and geographically closest relative, the omnivorous brown bear.

## Results

Multivariate rates of evolution for cranial shape are given in Table 1, where node numbers refer to nodes in Figure 1. The rate of skull shape evolution in the polar bear lineage was about double the mean rate observed for other parts of ursid phylogeny (mean ursid rate = 0.024, +/−0.007, polar bear rate = 0.059). This difference was significant based on a one-tailed T-test ($t_6$ = 4.92, $p$ = 0.0013).

Surface area to volume ratios for the finite element models of polar and brown bear skulls were similar, indicating that similar amounts of bone are used in the skulls of both species (SA/V: polar bear = 0.61, brown bear = 0.59). This finding suggests that differences in stress magnitudes between the polar bear and scaled brown bear skull models can be interpreted in light of differences in external shapes of the skulls. Bite forces measured from the two scaled finite element models were also comparable for all
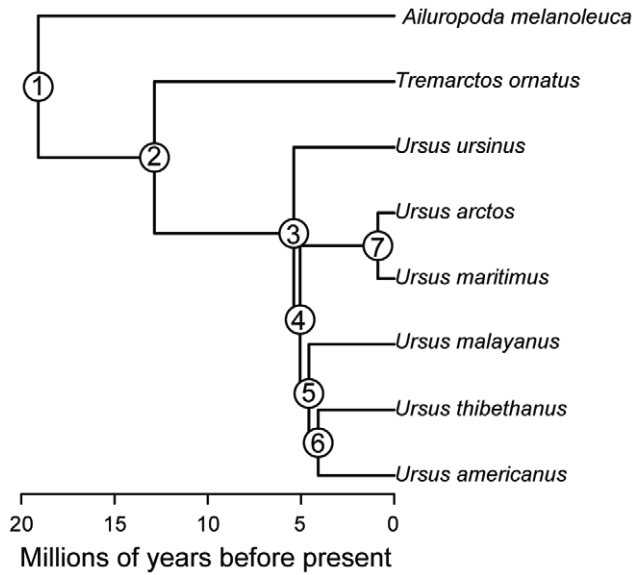
**Figure 1. Time-calibrated ursid phylogeny used for assessing rates of cranial shape evolution.** Node numbers correspond to those used for evolutionary contrasts (see Table 1).
doi:10.1371/journal.pone.0013870.g001

**Table 2.** Bite forces and strain energy density (SED) values for the two models under four simulated bites.

|  |  | Canine | PM4 | M1 | M2 |
|---|---|---|---|---|---|
| polar bear |  |  |  |  |  |
|  | Bite Force right | 1939.96 | 3798.69 | 4481.55 | 5041.65 |
|  | Bite Force left | 2302.09 | 3882.04 | 4426.24 | 5127.36 |
|  | mean Bite force | 2121.02 | 3840.36 | 4453.90 | 5084.50 |
|  | SED right | 2.38 | 2.36 | 1.91 | 2.03 |
|  | SED left | - | 1.98 | 2.17 | 2.03 |
|  | mean SED | 2.38 | 2.17 | 2.04 | 2.03 |
| brown bear | Bite Force right | 1731.92 | 3832.53 | 4197.82 | 4570.43 |
|  | Bite Force left | 1630.84 | 3644.36 | 4119.48 | 4768.38 |
|  | mean Bite force | 1681.38 | 3738.45 | 4158.65 | 4669.41 |
|  | SED right | 1.86 | 1.31 | 1.25 | 1.52 |
|  | SED left | - | 1.35 | 1.34 | 1.35 |
|  | mean SED | 1.86 | 1.33 | 1.30 | 1.44 |

Values are given for FE analyses conducted with bite points on the right and left sides, as well as means over both sides.
doi:10.1371/journal.pone.0013870.t002

simulated bites, although the polar bear's bite was slightly stronger in each case (Table 2, Fig. 2a). These results suggest that the potential leverage of the jaw muscle systems is also similar for the two species.

Stress distributions and magnitudes differed between the two models for all bites. For each biting scenario, the polar bear skull exhibited more widely varying stresses (Fig. 3) and higher peak stresses (Table 3) than for the brown bear. Differences between the two species were most marked for bites made with the molars, where peak stresses in the polar bear were up to 408% those of the brown bear (Table 3). Similarly strain energy values were higher in the polar bear cranium than for the brown bear for all bites (Table 2; Fig. 2b), indicating that the polar bear skull undergoes more deformation in producing similar bite forces. Again, differences between the polar and brown bear crania were most pronounced for bites made with the post-canine dentition, the main site for processing of ingested food. Our model results are

unvalidated by *in vivo* data and should be treated as estimates only. However, based on our findings, it appears that although the two species are similar in cranial size and have similar muscle leverage potential, the polar bear's skull is a weaker, less work-efficient structure, and does not appear well suited to dealing with large masticatory loads.

**Table 1.** Mulitvariate evolutionary contrasts for ursid cranial shape.

| Contrast | mulitvariate rate |
|---|---|
| *A. melanoleuca* / node 1 | 0.025 |
| *T. ornatus* / node 2 | 0.013 |
| *U.ursinus* / node 3 | 0.023 |
| *U. arctos* / node 4 | 0.032 |
| *U.malayanus* / node 5 | 0.030 |
| *U. thibethanus* / *U.americanus* | 0.018 |
| Ursid mean (sd) | 0.024 (0.007) |
| *U.maritimus* / node 7 | 0.059 |

Node numbers refer to nodes in Fig. 1.
doi:10.1371/journal.pone.0013870.t001
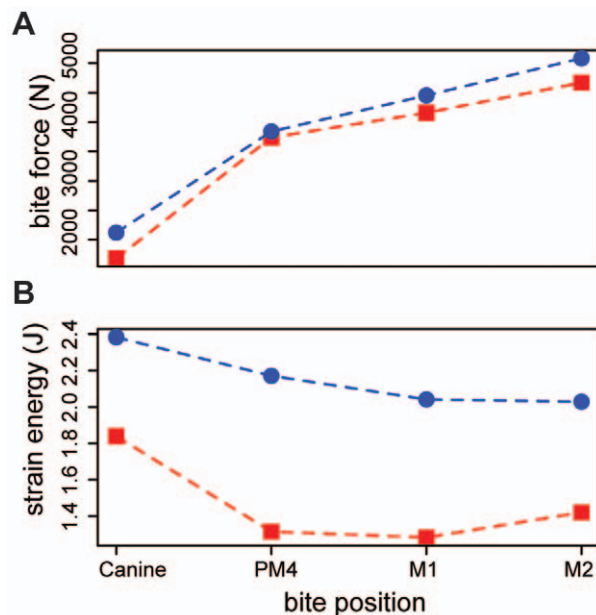


**Figure 2. Performance metrics assessed for four different bite positions in the polar bear (blue symbols) and brown bear (red symbols) FE models.** The *X* axis corresponds to bite point, with anterior bites towards the left and posterior bites to the right. Panel A shows bite forces, panel B shows cranial strain energy. Note that bite forces are similar in both species for all bites, while strain energies are uniformly lower in the brown bear.
doi:10.1371/journal.pone.0013870.g002

**Figure 3. FE models showing von Mises stresses in the polar bear (left) and brown bear (right) skulls during bilateral canine biting (A,E), and unilateral PM4 (B,F), M1 (C,G), and M2 (D,H) biting.**
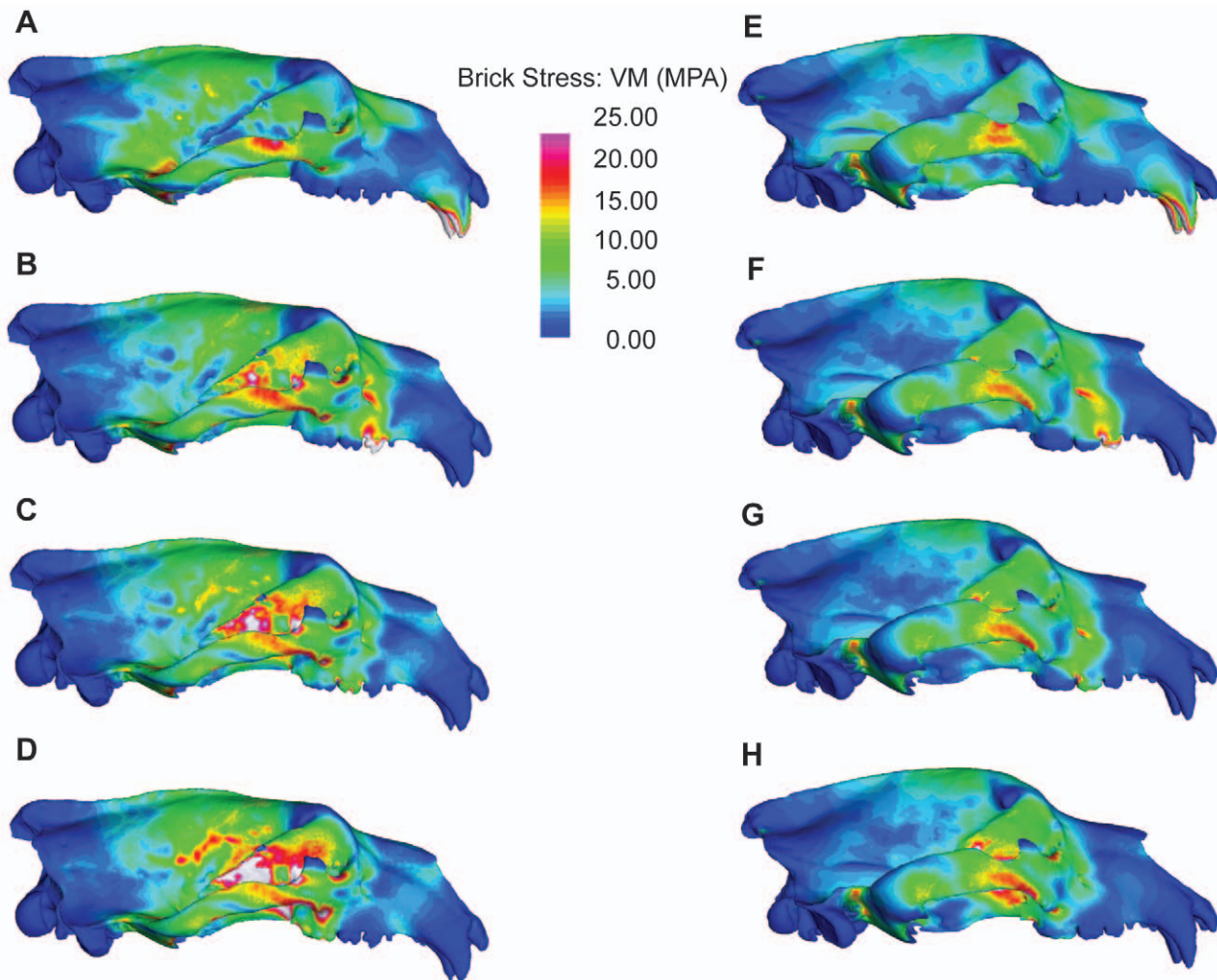doi:10.1371/journal.pone.0013870.g003

## Discussion

The transition to an arctic environment and hypercarnivorous diet resulted in extremely rapid morphological evolution in the polar bear lineage. Our results indicate that the rate of cranial shape evolution in the polar bear lineage was at least twice as fast as in other branches of ursid phylogeny. Our estimate is probably conservative; while the phylogeny that we used for rate estimates dates the polar bear/brown bear split at ~700 kya [3], recent analysis of sub-fossil polar bear remains suggests that polar bears diverged from brown bears as recently as 150 kya, and that the modern polar bear morphology was present by 130 kya [17]. Compared with other ursids, polar bears possess low flat skulls with elevated orbits [2], consistent with both semi-aquatic [18] and faunivorous [2] adaptations. This morphology might also increase hunting efficiency by allowing bears to thrust their heads into breathing holes or pupping dens. Polar bear evolution was facilitated by the expansion of polar ice sheets and floes in the late Pleistocene [19]. If polar bears evolved from coastal populations of brown bears [6], as molecular evidence now suggests [3–5], [17], then rapid evolution of adaptations for semi-aquatic life and hypercarnivory could have occurred to facilitate foraging over wider areas. Polar bears have denser fore- and hindlimb bones, a common adaptation of aquatic mammals, than closely related brown bears, further supporting this interpretation [20].

Although polar bears possess mechanically efficient skulls, as indicated by larger bite forces for a given muscle effort (Fig. 2A), we found that they also possess energetically inefficient and structurally weaker skulls (Fig. 2b; Fig. 3). This initially seems somewhat counterintuitive; among other carnivoran families, more carnivorous taxa tend to have stronger skulls [11], [13], [14]. However, polar bears feed almost exclusively on young ringed (*Pusa hispida*) and bearded (*Erignatus barbatus*) seals, which, at 68–250kg, are small prey in comparison to a ~500 kg adult polar bear [21], [22]. As a result, cranial reinforcement may not be necessary as in hypercarnivores such as lions or wolves that regularly take prey larger than themselves [11], [13], [14]. The performance of the polar bear skull is particularly poor during bites with the post-canine dentition. (Fig 2b; Fig 3b–d; f–h). Polar bears exhibit reduced premolars and molars in comparison with most other ursids [1] but also lack the well-developed shearing blade-like teeth of hypercarnivores [1], [23]. In this respect they parallel insectivorous carnivorans, such as aardwolf (*Proteles cristata*), bat-eared fox (*Otocyon megalotis*) and sloth bear (*Ursus ursinus*) [1], [2]. Although convergence between a carnivore and

**Table 3.** Peak Von mises stress for homologous cranial regions in the polar and brown bear models for the four simulated bites.

| bite position | skull region | polar bear | brown bear |
|---|---|---|---|
| bilateral canine | rt zygoma | 29.13 (7.95) | 26.46 (6.73) |
| | lt zygoma | 34.77(8.45) | 27.08 (6.60) |
| | palate | 24.49 (5.66) | 10.50 (2.94) |
| | snout | 13.49 (4.51) | 10.66 (4.59) |
| | frontal | 31.53 (6.32) | 11.66 (4.84) |
| | rt orbit | 27.72 (6.85) | 15.75 (5.13) |
| | lt orbit | 19.88 (7.32) | 21.40 (3.80) |
| PM4 | rt zygoma | 29.92 (9.30) | 21.02 (6.93) |
| | lt zygoma | 25.27 (5.65) | 19.17 (4.54) |
| | palate | 21.20 (5.12) | 9.94 (2.74) |
| | snout | 20.39 (2.76) | 14.41 (2.58) |
| | frontal | 24.39 (4.65) | 10.49 (4.03) |
| | rt orbit | 62.31 (15.37) | 20.23 (8.64) |
| | lt orbit | 14.07 (3.75) | 11.63 (2.02) |
| M1 | rt zygoma | 38.15 (9.79) | 22.84 (7.04) |
| | lt zygoma | 25.23 (6.08) | 19.16 (4.61) |
| | palate | 52.84 (6.76) | 16.10 (3.24) |
| | snout | 13.81 (2.66) | 13.94 (2.14) |
| | frontal | 22.9 (4.03) | 10.47 (3.85) |
| | rt orbit | 114.18 (23.22) | 27.93 (11.03) |
| | lt orbit | 21.84 (3.55) | 9.87 (1.84) |
| M2 | rt zygoma | 38.81 (9.92) | 27.26 (7.66) |
| | lt zygoma | 24.75 (4.63) | 18.80 (4.58) |
| | palate | 52.93 (6.51) | 17.93 (3.37) |
| | snout | 13.36 (2.63) | 10.99 (1.77) |
| | frontal | 22.92 (3.64) | 11.09 (3.83) |
| | rt orbit | 114.63 (23.16) | 45.72 (15.62) |
| | lt orbit | 22.09 (3.63) | 11.58 (1.81) |

Average brick stress for each region is also given in parentheses.
doi:10.1371/journal.pone.0013870.t003

insectivores also appears surprising, consideration of food material properties sheds light on this finding. Polar bears feed as almost exclusively on blubber and flesh that, unlike bone, require little or no processing prior to swallowing. If there is no selective advantage to maintaining large molars, they can be rapidly lost through the action of a few small mutations [24] or simple developmental mechanisms [25], [26]. Brown bears, in contrast, are generalized omnivores with unreduced dentitions [1], [2]. Although they consume animal protein when available, brown bears seasonally consume large amounts of plant material, including grasses, which require extensive mechanical breakdown and repeated skull loading prior to swallowing [27]. This is reflected in their larger molar grinding area, similar to other omnivorous ursids [1]. The lower peak stresses and higher work efficiency of the the brown bear cranium may result in part from the species' deep, vaulted and pneumatized forehead (see Fig. 3), a morphology that is characteristic of all herbivorous and omnivorous ursids [2]. Although pneumatized spaces are associated with reduced structural strength of the cranium [28], their presence is also associated with dissipation of regular, large peak masticatory

loads in bone-cracking hyaenas and fossil canids [29–32]. The low, flat head of the polar bear, while advantageous for its semi-aquatic lifestyle and hunting behavior, reduces the ability of the cranium to withstand repeated large loads generated by bites made with the post-canine dentition.

The polar bear has become a flagship species for global climate change in recent years. Projected climate trends in coming decades will have profound effects on polar bear populations by decreasing the availability of suitable denning sites as well as eliminating much of the polar sea ice over which this specialized ursid forages for its seal prey [33]. Furthermore, climate-driven northward expansion of temperate ecosystems and their associated faunas [34] has already begun to facilitate the movement of brown bears into polar bear territory [35]. The continued survival of the polar bear in the face of global climate change will ultimately depend on a range of factors, including behavioral and physiological flexibility. Our findings, combined with those of earlier studies, shed some light on the potential dietary flexibility of polar bear. In response to a specialized diet of seal blubber, polar bears rapidly lost the large grinding molars and deep vaulted skull that characterize omnivorous ursids. This has not only resulted in a dentition that is less suited to diets requiring high levels of oral food processing but also, based on our results, a cranium that is less suited to bearing the associated loads. Small differences in cranial stress and strain are probably not alone sufficient to force a species to extinction. However, increased competition from northward advancing brown bear populations will also present a significant challenge. In areas where specialized arctic foxes (*Vulpes lagopus*) overlap with more generalized red foxes (*Vulpes vulpes*), red foxes actively displace arctic foxes and control prime feeding and denning areas [36], [37]. In this context, even the slight selective advantage provided by the superior mechanical performance of the brown bear's cranial shape, combined with a loss of molar grinding area, could be enough in such a setting to contribute to the exclusion of the polar bear. As a consequence of exceptional rapid specialization to a high arctic diet of seal flesh, the polar bear appears to have lost the generalized feeding abilities of its close relative. As a result, if current climate trends continue, one of the most striking examples of rapid phenotypic evolution may be lost as quickly as it appeared.

## Materials and Methods

### Rates of Cranial Shape Evolution

We computed multivariate rates of cranial shape evolution following [7]. Our morphometric data comprised mean principal component scores from a previous study of cranial shape variation across all extant ursid species [2]. We calculated rates of evolution from these data on an ursid phylogeny (Fig. 1) with topology and branch lengths from [3]. The rate of cranial shape evolution in the polar bear lineage was compared to the distribution of rates in other ursids using a one-tailed T-test. Analyses were conducted with R 2.10.1 [38] using custom-written scripts and functions from the APE [39] and Geiger [40] packages.

### Creating skull models

Dry skulls of one adult male polar bear (Illinois State Museum H001-05) and one adult male brown bear (United States National Museum 82003) were CT scanned at the High Resolution CT facility at the University of Texas, Austin. Slice thickness/inter-slice spacing was 0.75mm (polar bear) and 1mm (brown bear). Both scans are available via the digital morphology website (http://www.digimorph.org). Due to the high cost of CT scanning and the time consuming nature of FE model construction, only

one specimen per species was used. Both specimens were quantitatively typical for their species based analysis of landmark data following [2]. Skulls were assessed as adult based on tooth eruption and full closure of the basilar synchondrosis.

3D surface models of the crania were rendered in AMIRA v.4.1.2-1 (Visualization Sciences Group, Massachusetts, USA). An automated thresholding tool was initially used to delimit bone surfaces. We then manually edited the slices. At this stage we made a number of simplifying steps to reduce model complexity. First, we omitted the complex turbinal bones within the nasal cavity and semi-circular canals of the middle ear, as these presumably do not function in load bearing. We also simplified the morphology of complex structures that can be problematic in FE modeling, such as the perforated cribriform plate of the ethmoid. Second, we modeled teeth as continuous with surrounding maxillary bone as in other FE studies [9–11], [13], [14], [41]. Although tooth roots and periodontal ligaments (PDL) play important roles in transmitting and absorbing forces, recent work suggests that inclusion of the PDL in finite element models affects only local strain in the region of the alveolus [42] and so presumably does not affect global patterns of performance. Third, we ignored the distribution of trabecular bone and modeled the entire cranium as continuous cortical bone. Although this will over-stiffen the models, both contained similar amounts of cancellous bone and so are presumably affected in similar ways. Finally, we omitted to model the intricate three-dimensional morphology of cranial sutures. Recent FE work suggests that sutures may play important roles in locally reducing strain in non-mammalian tetrapod skulls [43], [44] but their significance in mammalian cranial function remains to be explored. Internal cavities, such as the frontal sinuses and tympanic bulla cavity were modeled as hollow, preserving potential biomechanical function. Simplified skull models were imported into Geomagic Studio v.10. (Geomagic Corp. North Carolina, USA), where we manually edited the surfaces to correct artifacts of the reconstruction process and patch holes. Once watertight surface models of the two skulls had been created, we re-exported them for FE modeling.

## Finite Element models

The complete, simplified skull models were imported into Strand7 (Strand7 Pty. Ltd., Sydney, Australia) for FE analysis. We created Finite Element meshes of the cranium only (the mandible was retained only for positioning muscle vectors) using 4-noded tetrahedral elements. The final models comprised 841,531 elements for the polar bear and 984,184 elements for the brown bear. Complete finite element models have been deposited with, and are available for download from Biomesh (http://www.biomesh.org/models). Ideally, we would have assigned complex material properties to our models to account for regional variation in the distribution of cortical and cancellous bone, and the orthotropic material behavior of bone. Because the use of homogenous material properties in FEMs has been shown to produce surface strains that fall within the range of values of obtained from *in vivo* strain gauge studies [45] and material properties are currently not available for polar or brown bear cranial bone, we made the simplifying assumption here to assign homogeneous isotropic material properties based on values for domestic dog cortical bone, following [46], [47] (E = 13.7 GPA, ν = 0.3). Our study is not validated and thus absolute values of results should be treated with caution. However, as the aim of our study is comparative and both skulls were modeled in identical ways, we should still be able to draw broad conclusions regarding comparative performance of the skulls of the two species from the results obtained.

## Muscle forces

We applied muscle forces over the origins of the temporalis, masseter and pterygoideus (internal+external) muscles using the tangential-plus-normal traction model in the program BoneLoad [15]. This method incorporates the effects of muscle wrapping around curved bone surfaces and eliminates artifacts caused by point loads in areas of muscle insertion. A thin layer of plates $(10^{-4}\text{mm})$ was applied over the entire area of muscle origin for each muscle. The plates were assigned the same material properties as the tetrahedral elements forming the cranium. Muscle forces were then applied to the plate surfaces. To provide focal points for the muscle forces to act towards, we identified the *x,y,z* coordinates of nodes on the mandibles representing the estimated center points of the temporalis, masseter, and pterygoideus insertion areas. We subsequently deleted the plates constituting the mandibles and, in their place, created six nodes at the exact co-ordinates of the previously identified focal positions for the muscles. These newly created nodes were used as focal points for the action of the muscle forces. For example, all left temporalis forces pulled towards a focal node representing the center point of temporalis insertion on the left mandible.

Measurements of cross section area of the jaw muscles were not available for the species modeled here. Instead, a total amount of muscle force (see below) was distributed in each model according to percentage contribution of temporalis (65.17%), masseter (28.08%) and pterygoideus (6.75%) to total jaw muscle mass in the closely related American black bear *Ursus americanus* [48]. Available evidence suggests that these values are consistent across such disparate carnivoran families as felids and canids [48], [49]. During biting with the post-canine dentition, jaw muscles are likely to differ in activity patterns on working and balancing sides of the jaw. To ensure that the assumption of maximal muscle activity did not bias our results, we conducted analyses at the post-canine dentition with forces allocated at a 1:0.66 ratio between working and balancing sides, based on electromyographic work on the domestic dog [50] and subsequent FE studies of carnivoran mastication [31].

## Constraints

To prevent free-body rotation (unconstrained movement of models in space), we followed protocols described in [45]. We constrained a single node at each glenoid fossa, creating a virtual axis of rotation with the ventrally directed muscle forces rotating the cranium about the temporal-mandibular joint. To simulate biting behavior and measure feeding performance (i.e. bite force, cranial stress and strain), we applied additional single node constraints at teeth involved in the simulated biting behaviors. This added a virtual bite point, with the rotating skull meeting a point of resistance at the bite point and a resultant virtual bite force generated. From this action, resultant stresses and strain can be calculated and visualized. We simulated four bite scenarios that ursids use when feeding: a bilateral canine bite (one constrained node at the tip of each canine); and unilateral bites at the fourth upper premolar - the "carnassial" (a single constrained node at the carnassial notch); upper first molar (a single constrained node at the protocone); and upper second molar (a single constrained node at the protocone). To ensure that asymmetries in the models and placement of constraints did not influence results, we repeated analyses for both left and right teeth and averaged subsequent bite force and strain energy results (Table 2).

## Scaling and Assessing Performance

We controlled for differences in size between the models using a recently developed method for comparing FE models [16]. In order

to ensure that stress values are comparable among models of different sizes, it is important that force to surface area ratios are constant among finite element models. Therefore, prior to analysis, both models were scaled to common surface area corresponding to that of the polar bear model (1,209,042 mm$^2$). To produce realistic estimates of bite force we used the total muscle force derived from a dry skull estimate of the cross sectional area of temporalis and masseter plus pterygoideus muscles in the polar bear (18069.6 N - [51]). For bilateral canine bites, this total muscle force was distributed according to proportions described above from the black bear. For unilateral post-canine bites, we reduced the balancing side muscle forces by 2/3, resulting in a working side total of 9034.8 N and a balancing side total of 6023.2 N.

We evaluated performance of the models based on three criteria. First, we determined how skull shape affects bite performance by comparing bite forces at the constrained nodes on the teeth. Because all models were scaled to a common surface area and used equal muscle forces, our null hypothesis was that bite forces should be identical among the models. Any differences in bite forces could then be interpreted as the result of differences in skull geometry alone [16]. Second, we assessed strength of the skull models by comparing model stress, measured as Von Mises stress [9]. Bone is an elastic material and therefore fails under a ductile, rather than brittle model of fracture [52]. Von Mises stress is a scalar function of the principle stresses at each element and provides a good predictor of failure due to ductile fracture [9]. Lower peak stress values and more even stress distributions were interpreted as indicating a stronger structure for a given loading condition. Finally, we assessed the work efficiency of the skull models by comparing total strain energy values, a measure of energy lost to deformation. In terms of work efficiency, efficient structures are those that maximize stiffness for a given volume of material [16]. Lower strain energy values indicate stiffer structures and therefore greater work efficiency. Strain energy values were corrected for differences in volumes of the models using Equation 5 from Dumont et al. [16]. Our null hypotheses for all analyses were that stress and strain energy values should be identical among scaled models. All FE analyses were linear static and were completed in Strand7.

## Author Contributions

Conceived and designed the experiments: GJS. Performed the experiments: GJS LL PY. Analyzed the data: GJS BF LL PY. Contributed reagents/materials/analysis tools: GJS BF BVV. Wrote the paper: GJS BF BVV.

## References

1. Sacco T, Van VB (2004) Ecomorphological indicators of feeding behaviour in the bears (Carnivora: Ursidae). J Zool 263: 41–54.
2. Figueirido B, Palmqvist P, Perez-Claros JA (2009) Ecomorphological correlates of craniodental variation in bears and paleobiological implications for extinct taxa: an approach based on geometric morphometrics. J Zool 277: 70–80.
3. Krause J, Unger T, Nocon A, Malaspinas AS, Kolokotronis SO, et al. (2008) Mitochondrial genomes reveal an explosive radiation of extinct and extant bears near the Miocene-Pliocene boundary. BMC Evol Biol 8: 220.
4. Talbot SL, Shields GF (1996) Phylogeography of brown bears (Ursus arctos) of Alaska and paraphyly within the Ursidae. Mol Phylogenet Evol 5: 477–494.
5. Barnes I, Matheus P, Shapiro B, Jensen D, Cooper A (2002) Dynamics of Pleistocene population extinctions in Beringian brown bears. Science 295: 2267–2270.
6. Kurtén B (1964) The evolution of the polar bear Ursus maritimus. Acta Zoologica Fennica 108: 1–30.
7. McPeek MA, Shen L, Torrey JZ, Farid H (2008) The tempo and mode of three-dimensional morphological evolution in male reproductive structures. Am Nat 171: E158–E178.
8. Rayfield EJ (2004) Cranial mechanics and feeding in Tyrannosaurus rex. Proc R Soc London B 271: 1451–1459.
9. Dumont ER, Piccirillo J, Grosse IR (2005) Finite-element analysis of biting behavior and bone stress in the facial skeletons of bats. Anat Rec A 283: 319–330.
10. McHenry CR, Wroe S, Clausen PD, Moreno K, Cunningham E (2007) Supermodeled sabercat, predatory behavior in Smilodon fatalis revealed by high-resolution 3D computer simulation. PNAS 104: 16010–16015.
11. Wroe S, Clausen P, McHenry C, Moreno K, Cunningham E (2007) Computer simulation of feeding behaviour in the thylacine and dingo as a novel test for convergence and niche overlap. Proc R Soc London B 274: 2819–2828.
12. Strait DS, Weber GW, Neubauer S, Chalk J, Richmond BG, et al. (2009) The feeding biomechanics and dietary ecology of Australopithecus africanus. PNAS 106: 2124–2129.
13. Slater GJ, Dumont ER, Van VB (2009) Implications of predatory specialization for cranial form and function in canids. J Zool 278: 181–188.
14. Slater GJ, Van VB (2009) Allometry and performance: the evolution of skull form and function in felids. J Evolution Biol 22: 2278–2287.
15. Grosse IR, Dumont ER, Coletta C, Tolleson A (2007) Techniques for modeling muscle-induced forces in finite element models of skeletal structures. Anat Rec A 290: 1069–1088.
16. Dumont ER, Grosse IR, Slater GJ (2009) Requirements for comparing the performance of finite element models of biological structures. J Theor Biol 256: 96–103.
17. Lindqvist C, Schuster SC, Sun YZ, Talbot SL, Qi J, et al. (2010) Complete mitochondrial genome of a Pleistocene jawbone unveils the origin of polar bear. PNAS 107: 5053–5057.
18. Howell AB (1930) Aquatic mammals: Their adaptations to life in the water. Springfield: Charles C. Thomas Publishing.
19. Lister AM (2004) The impact of Quaternary Ice Ages on mammalian evolution. Philos Trans R Soc B 359: 221–241.
20. Wall WP (1983) The correlation between high limb-bone denisty and aquatic habits in recent mammals. J Paleontol 57: 197–207.
21. Stirling I, Archibald WR (1977) Aspects of predation of seals by polar bears. J Fish Res Board Can 34: 1126–1129.
22. DeMaster DP, Stirling I (1981) Ursus maritimus. Mamm Spec 145: 1–7.
23. Evans AR, Wilson GP, Fortelius M, Jernvall J (2007) High-level similarity of dentitions in carnivorans and rodents. Nature 445: 78–81.
24. Kangas AT, Evans AR, Thesleff I, Jernvall J (2004) Nonindependence of mammalian dental characters. Nature 432: 211–214.
25. Kavanagh KD, Evans AR, Jernvall J (2007) Predicting evolutionary patterns of mammalian teeth from development. Nature 449: 427–U1.
26. Polly PD (2007) Evolutionary biology - Development with a bite. Nature 449: 413–415.
27. Rode KD, Robbins CT, Shipley LA (2001) Constraints on herbivory by grizzly bears. Oecologia 128: 62–71.
28. Farke AA (2008) Frontal sinuses and head-butting in goats: a finite element analysis. J Exp Biol 211: 3085–3094.
29. Werdelin L (1989) Constraint and adaptation in the bone-cracking canid Osteoborus (Mammalia: Canidae). Paleobiology 15: 387–401.
30. Tanner JB, Dumont ER, Sakai ST, Lundrigan BL, Holekamp KE (2008) Of arcs and vaults: the biomechanics of bone-cracking in spotted hyenas (Crocuta crocuta). Biol J Linn Soc 95: 246–255.
31. Tseng ZJ (2009) Cranial function in a late Miocene Dinocrocuta gigantea (Mammalia: Carnivora) revealed by comparative finite element analysis. Biol J Linn Soc 96: 51–67.
32. Joeckel RM (1998) Unique frontal sinuses in fossil and living Hyaenidae (Mammalia, Carnivora): Description and interpretation. J Vert Paleo 18: 627–639.
33. Derocher AE, Lunn NJ, Stirling I (2004) Polar bears in a warming climate. Integr Comp Biol 44: 163–176.
34. Parmesan C, Yohe G (2003) A globally coherent fingerprint of climate change impacts across natural systems. Nature 421: 37–42.
35. Rockwell R, Gormezano L, Hedman D (2008) Grizzly Bears, Ursus arctos, in Wapusk National Park, Northeastern Manitoba. Can Field Nat 122: 323–326.
36. Killengreen ST, Ims RA, Yoccoz NG, Brathen KA, Henden JA, et al. (2007) Structural characteristics of a low Arctic tundra ecosystem and the retreat of the Arctic fox. Biol Conserv 135: 459–472.
37. Tannerfeldt M, Elmhagen B, Angerbjorn A (2002) Exclusion by interference competition? The relationship between red and arctic foxes. Oecologia 132: 213–220.

38. R Development Core Team (2010) R: A Language and Environment for Statistical Computing. Vienna, Austria. ISBN 3-900051-07-0, URL http://www.R-project.org.

39. Paradis E, Claude J, Strimmer K (2004) APE: Analyses of Phylogenetics and Evolution in R language. Bioinformatics 20: 289–290.

40. Harmon LJ, Weir JT, Brock CD, Glor RE, Challenger W (2008) GEIGER: investigating evolutionary radiations. Bioinformatics 24: 129–131.

41. Wroe S (2008) Cranial mechanics compared in extinct marsupial and extant African lions using a finite-element approach. J Zool 274: 332–339.

42. Panagiotopoulou O, Kupczik K, Cobb SN (2010) The mechanical function of the periodontal ligament in the macaque mandible: a validation and sensitivity study using finite element analysis. J Anat.

43. Moazen M, Curtis N, O'Higgins P, Jones MEH, Evans SE, et al. (2009) Assessment of the role of sutures in a lizard skull: a computer modelling study. Proc R Soc London B 276: 39–46.

44. Jasinoski SC, Rayfield EJ, Chinsamy A (2010) Mechanics of the scarf premaxilla-nasal suture in the snout of *Lystrosaurus*. J Vert Paleont 30: 1283–1288.

45. Strait DS, Wang Q, Dechow PC, Ross CF, Richmond BG, et al. (2005) Modeling elastic properties in finite element analysis: How much precision is needed to produce an accurate model? Anat Rec A 283A: 275–287.

46. Cook SD, Weinstein AM, Klawitter JJ (1982) A 3-dimensional finite-element analysis of a porous rooted CO-CR-MO alloy dental implant. J Dent Res 61: 25–29.

47. Verrue V, Dermaut L, Verhegghe B (2001) Three-dimensional finite element modelling of a dog skull for the simulation of initial orthopaedic displacements. Eur J Orthodont 23: 517–527.

48. Davis DD (1955) Masticatory apparatus in the spectacled bear *Tremarctos ornatus*. Fieldiana: Zoo 37: 25–46.

49. Turnbull WD (1970) Mammalian masticatory apparatus. Fieldiana: Geol 18: 149–356.

50. Dessem D (1989) Interactions between jaw-muscle recruitment and jaw joint forces in *Canis familiaris*. J Anat 164: 101–121.

51. Christiansen P, Adolfssen JS (2005) Bite forces, canine strength and skull allometry in carnivores (Mammalia, Carnivora). J Zool 266: 133–151.

52. Nalla RK, Kinney JH, Ritchie RO (2003) Mechanistic fracture criteria for the failure of human cortical bone. Nat Mater 2: 164–168.